Adam Czajka, Przemek Strzelczyk, "Iris recognition with compact zero-crossing-based coding", in: Ryszard S. Romaniuk (Ed.), *Proceedings of SPIE - Volume 6347, Photonics Applications in Astronomy, Communications, Industry, and High-Energy Physics Experiments 2006*, 634723, Oct. 12, 2006 (doi: 10.1117/12.714578)

Iris recognition with compact zero-crossing-based coding

Adam Czajka, *Member, IEEE,* and Przemek Strzelczyk

Biometrics Laboratory, Research and Academic Computer Network NASK, Warsaw, Poland
Warsaw University of Technology, Warsaw, Poland

ABSTRACT

We propose an iris recognition technique using transformation of the iris image into a binary sequence that represents zero-crossing points of the filtered image by way of Laplacian of Gaussians. Novel iris localization and occlusion detection methods are developed to transform the iris image into the sequence of 1D stripes. The proposed enrollment procedure includes an independent selection of iris stripes among a number of enrollment images to minimize the recognition errors. The eyeball spontaneous rotation is corrected at the verification stage. The methodology was tested with a local database of 180 different irises, revealing the EER (*Equal Error Rate*) at the level of 0.03%.

Keywords: iris recognition, zero-crossing, biometrics.

INTRODUCTION

Biometric researchers are still looking for "ideal biometrics". This paragon may be visualized as a physical or behavioral characterization of a person and a method of its symbolic description, fused in a system that is resistant to counterfeits, produces no authentication errors, is immune to aging and diseases, brings no social, religious, ethical, and other objections, and finally, is comfortable in use.

Iris-based authentication is important candidate for being a source of highly distinctive attributes characterizing identity with a high accuracy. It is fast, highly reliable and, by its nature, non-invasive. The structure of iris muscle, used in recognition, is stable throughout the human life and it is independent of a human genotype [3,4]. Also, the iris recognition raises little social objections. Although there is a wide variety of biometric modalities that have been investigated and applied to various access control scenarios, iris biometrics seems to be close to ideal and is likely to prevail over its competitors.

The iris texture complexity is very high and may need non-trivial feature extraction, coding algorithms and large computation times. The iris authentication methodology has been pioneered by John Daugman. He was the first who proposed an automatic iris recognition methodology based on Gabor filtering, patented in 1987 [3]. Presently, most of the commercial solutions are based on Daugman's algorithms. Nevertheless, iris recognition is not a solved task, and there is a sustaining demand for new solutions, aiming at fast and robust iris tracking, localization and feature extraction.

In this paper we propose a new method of iris texture coding and feature extraction based on localization of zero-crossing points of the filtered iris image and their appropriate representation and processing.

2. IRIS MEASUREMENT

2.1 EYE IMAGING

Before any type of processing, the iris images must first be captured. A special hardware was designed and constructed, called Iris Imaging Device (IID), to manage the iris image capture process from a convenient distance and with minimal human cooperation. Constructing the device capable of taking iris pictures quickly showed that various technical problems had to be overcome, as related, for instance, to spontaneous movements of the human eye, small depth-of-field and a finite patience of volunteers, which limits the capture time to a few seconds. It is noteworthy that the application of commercial biometric devices for iris imaging purpose only is difficult since in almost all cases a measuring device is inseparably connected to a particular authentication methodology.

IID consists of a camera with active optics, infrared illuminators, positioning mirrors and LEDs. The latter elements allow making the IID interactive with a volunteer during the imaging process. This helps to position volunteer's head correctly behind the optics. Once the hardware encounters the eye existence in a proper distance and position, it automatically starts to acquire a sequence of frames with varying focal length, thus compensating small depth-of-field that is common in imaging small targets as the human iris. The acquisition process takes approximately one second, and the whole iris image capturing including eye positioning approximates to 5 seconds. An example iris image captured by IID is illustrated in Fig. 1. The iris images are compliant with the rectilinear iris image requirements as published in ISO/IEC 19794-6 Final Committee Draft [1].

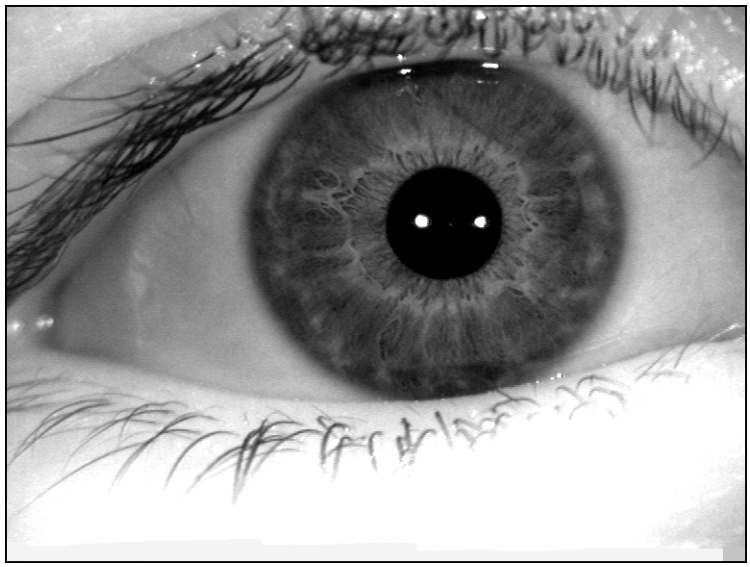

Figure 1. Example of raw iris image captured by IID

IID is a part of Iris Recognition System prototype and was also used to create a multimodal biometric database - BioBase, which at present contains images of iris, face, hand, fingerprints and handwritten signatures, of couple of hundred volunteers. BioBase will be employed here to test the proposed compact zero-crossing-based coding.

2.2 IRIS LOCALIZATION

Camera raw image contains the iris and its surroundings, Fig. 1. Additionally, the iris body is almost always occluded by eyelids, eyelashes, or interfered by specular reflections as a result of infrared illumination. Thus, the iris must be *localized* to extract the iris texture information. We define *localization* as the calculation of a certain set of parameters which allow unambiguous classification of image pixels into the iris and non-iris classes. These parameters are a) pupil

and limbus center coordinates and radii, b) a map of occlusions, and both sets of parameters are determined in two consecutive stages.

In the first stage, we make use of local image gradient estimation to outline of both inner (i.e., between the pupil and the iris) and outer (i.e., between the iris and the sclera) iris boundaries. The shape of inner and outer boundaries is approximated by two non-concentric circles.

In the second stage of iris localization we look for the iris occlusions. Collected iris images show that the eyelid boundary is often highly disrupted by protruding eyelashes preventing in some cases unambiguous eyelid detection. Thus we propose a routine that does not assume any particular occlusion shape and allows localizing irregular disruptions like eyelashes or reflections. The method makes use of local non-uniformity value determined within the ring outlined by the inner and outer iris boundaries. A set of angular directions is constructed, originating from the iris center, in which the iris texture is analyzed between the inner and outer boundaries. Additionally, the maximal allowed non-uniformity value is determined for the directions in which the probability of iris coverage is minimal. Directions in which the local non-uniformity of the analyzed iris texture exceeds the maximum value point the occlusion discrete angle. To finally obtain the map of occlusions, a discrete set of analysis directions is selected along with the corresponding radial positions of the local inconsistencies of the iris body. Figure 2 presents the camera raw image with iris boundaries and eyelid occlusions localized.

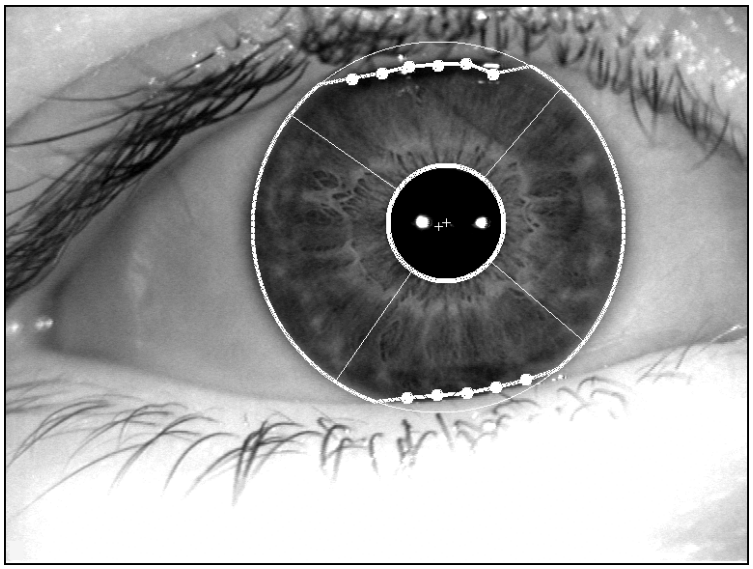

Figure 2. Same as in Fig. 1 with pupil and limbus boundaries determined.
A map of occlusions (white circles) automatically set, is also shown.

2.3 ASSESSMENT OF THE IRIS IMAGE QUALITY

In order to ascertain whether the acquired image is of the required quality (in terms of focus and iris body availability), two image attributes are investigated: focus factor and the iris body coverage by eyelids. These attributes are the basis for separate “experts” judging on the image quality, and giving a binary decision whether the image passed the test. It is assumed that image quality (from the iris recognition perspective) is sufficient if both experts positively classify the image.

2.3.1 Focus factor

The requirement of an image quality check based on frequency analysis was addressed by Daugman [4] and Ma *et al.* [5]. It is difficult to define the degree of image “blurriness” that may be the basis for image rejection and abandoning further processing. The exact criterion can be given only when the requirements are back-propagated to the image space

from the requirements imposed on the resulting features. This is because features extraction is always "sensitive" to a particular frequency band. Thus, image blurriness may be "invisible" to feature extraction, i.e. it may have no influence on the determined features if the frequency of analysis functions is significantly lower than the frequency disregarded due to blurring in the original image.

Iris focus-based quality is validated within the iris body rather than in the entire image. This is possible once the pupil is localized. Since it is relatively difficult to introduce a quality criterion, it is estimated experimentally. Images which, due to the blur, do not contain the projection of the iris muscle fibers layout, which typically can be observed, are selected to represent low quality iris images. The method relies on windowing the image power spectrum for two frequency bands: one representing the most common frequency observed for all iris images, and the other representing the camera noise. The quotient of the resulting cumulative amplitudes for both windows depends on the signal-to-noise ratio, thus estimating the image quality. The appropriate acceptance threshold value is set experimentally with the use of local database of iris images.

2.3.2 Iris body coverage

The second iris image quality determinant relies on the presence of non-occluded iris body. Since two iris sectors are used in further processing, it is necessary to ensure that both sectors are free of occlusions. The iris image passes the test if it is possible to inscribe both iris sectors within its body that does not contain any point of the occlusions map, automatically localized using the non-uniformity detection method.

Typically, during system operation, if the image quality is too low (at least one "expert" rejects the image), the reason for failure is passed to the volunteer by the device, so as to improve the image quality in the next approach. Figure 3 indicates example images which were automatically rejected due to a failure of two different image quality "experts" discussed in this subsection.

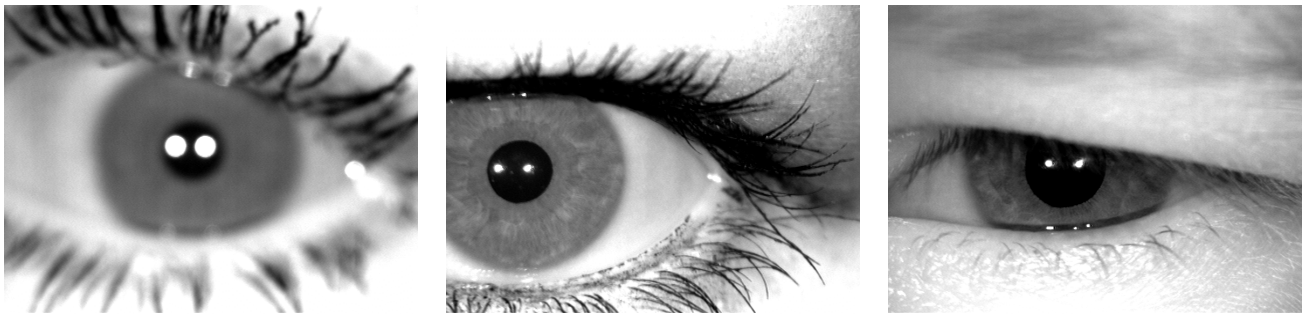

Figure 3. Example iris images that *did not* pass the quality check due to:
low focus factor (left) or frame (middle) and eyelids (right) coverage.

2.4 IRIS BODY REPRESENTATION

Based on localized occlusions, one may select two independent iris sectors, each of 90^o in width, to be further used in the analysis. The choice of angular width is based on observations with the local iris image database, and this represents the value of angular width that is available in average for collected images. Since the volunteers were not forced to open their eyes in a particular way during capture, it is concluded that once the eyelid coverage is too high, the system may ask for the eye to be opened more widely to finally extract two such sectors with minimal effort by the user. Since both sectors are dynamically inscribed into the iris body depending on the occlusion coverage, the angles defining the angular position of both sectors are in consequence inseparable elements of the iris template.

Due to the natural, circular shape of the iris, our approach uses a polar iris image representation. Spontaneous pupil constrictions that are typical to the eye physiology, we compensate for pupil radius changes as proposed by Daugman [3]. Since the iris and the pupil are not concentric, one of possible transformations of the iris image into non-concentric polar coordinates is used.

The experiments (see also [3,4]) revealed a much higher correlation of the iris body in the radial direction as compared to the angular direction. Thus the radial direction is analyzed more sparsely than the angular one. For each sector, we use R=16 different radii and N=512 different discrete angles to finally end up with polar representation of both iris sectors. Consequently, the iris free-of-occlusion sectors localized automatically is divided into $2R$ discrete functions each N point length. These functions are called *iris stripes*, since each one represents the iris texture information within the "stripe" of the original iris image. Iris stripes form the input information for zero-crossing-based coding employed in this work. Figure 4 presents both iris sectors in polar coordinates (iris stripes) as determined for the iris image illustrated in Fig. 1.

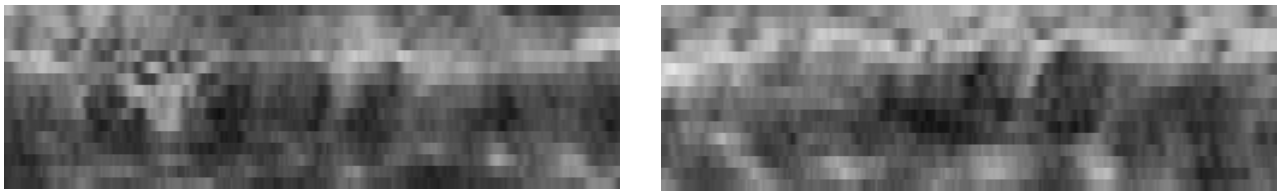

Figure 4. Iris stripes automatically determined for the iris image shown in Fig. 1.

3. IRIS CODING

We treat iris stripes as one-dimensional signals and decompose them at different resolution levels. The aim is to capture the identity discriminative information from the signal, simultaneously filtering out the noise, which is always present in iris imaging. Inspired by Boles, we applied a scaled Laplacian of Gaussians as a filtering function. In order to reduce the feature vector, and computation effort we limited the number of filter resolutions to four to achieve the best verification performance. For simplification, each filtered stripe will be called *f-stripe*. Note that having $2R$ iris stripes and 4 different filters, we obtain $8R$ f-stripes in total (for one eye). All f-stripes are consequently transformed into the sequence of positions of zero-crossing points.

We compare two methods of representation of the zero-crossings. The first one, proposed earlier by Boles, holds the coordinates of the zero-crossings and average function values between each two consecutive zero-crossings. We call it *rectangular representation* since this allows us to reconstruct f-stripes in rectangular form, Fig. 6 (middle). In the second approach, introduced by these authors, we quantize the f-stripe by way of one bit only, thus being constructing a limited version of a rectangular representation. We call this second approach *sign-only representation,* which is the *compact version* of the original zero-crossing-based method.

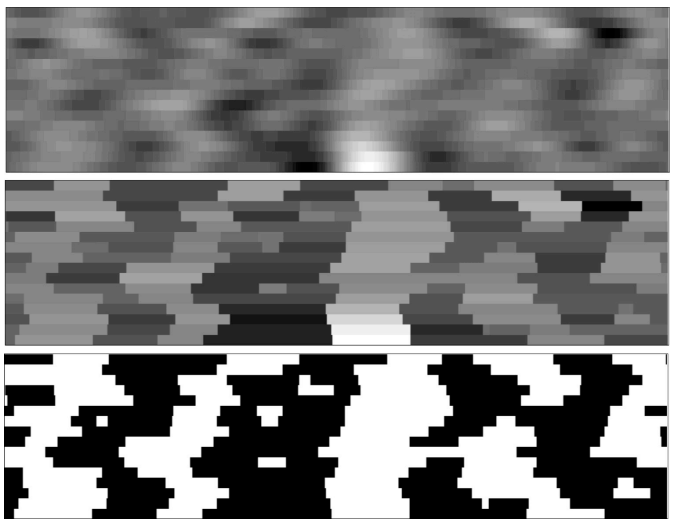

Figure 5. Image of f-stripes (top), rectangular reconstruction of the f-stripes (middle) and sign-only reconstruction of the f-stripes (bottom)

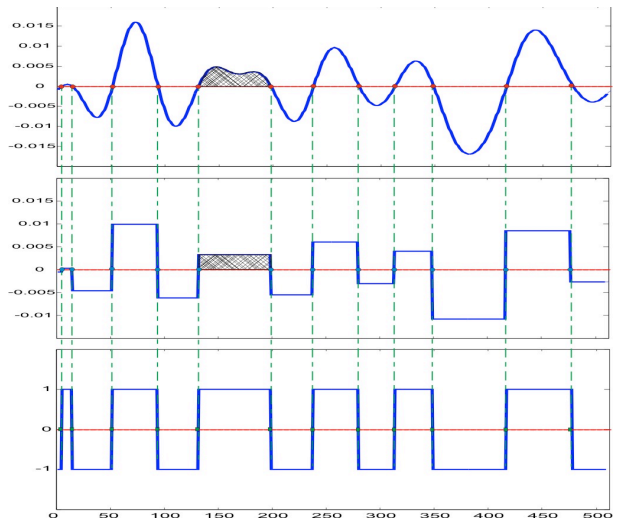

Figure 6. Same as in Fig 5, except one f-stripe is illustrated (top), along with its rectangular reconstruction (middle), and its sign-only reconstruction (bottom)

Consequently, in rectangular representation, we understand a single *iris feature* as the position of the zero-crossing along with the value of average intensity of the filtered stripe between the actual and the next zero-crossing point. In turn, in sign-only representation, the iris feature is simplified to the position of the zero-crossing point merged with the sign of the filtering result.

The size of the iris template is typically 15-20kB (rectangular representation) and 2-4kB (sign-only representation), depending on the number of localized zero-crossings.

4. IRIS RECOGNITION

4.1 PARTIAL MATCHING

Matching for both iris feature representations differs. We describe how to assess the dissimilarity between two f-stripes originating from different images. This is a crucial element of the iris matching used in the proposed methodology.

Let $t_{s,f}$ and $v_{s,f}$ denote the rectangular reconstructions of the f-stripe s filtered with filter f for two different image t and v, respectively. A partial matching score $S^{rect}_{s,f}(t,v)$ is based on correlation, namely:

$$S^{rect}_{s,f}(t,v) = \min(\widehat{S}^{rect}_{s,f}(t,v), \widehat{S}^{rect}_{s,f}(v,t)) \tag{4.1}$$

where

$$\widehat{S}^{rect}_{s,f}(y,z) = \min_{m\in[0,M]} 1 - \frac{\sum_{x=m}^{N-M+m} y_{s,f}(x) z_{s,f}(x+m)}{||y_{s,f}||||z_{s,f}||} \frac{N}{N-|m|}$$

and $|\,x\,|$ denotes an absolute value of x, $\|\,x\,\|$ corresponds to the root square of the total energy of x, N denotes the f-stripe length and M is the maximal allowed shift for eyeball rotation correction routine. Minimization in (4.1) with respect to shift between the compared f-stripes is introduced to compensate for the eyeball rotation that is typically present in the source images.

Now, let $t^*_{s,f}$ and $v^*_{s,f}$ denote the sign-only reconstructions of the f-stripe s filtered with filter f for two different image t and v, respectively. We can calculate a partial matching score $S^{sign}_{s,f}(t,v)$ in case of using sign-only reconstruction of f-stripes in a similar way to calculating $S^{rect}_{s,f}$, namely

$$S^{sign}_{s,f}(t,v) = \min(\widehat{S}^{sign}_{s,f}(t^*,v^*), \widehat{S}^{sign}_{s,f}(v^*,t^*)) \tag{4.2}$$

where

$$\widehat{S}^{sign}_{s,f}(y^*,z^*) = \min_{m\in[0,M]} 1 - \frac{\sum_{x=m}^{N-M+m} y^*_{s,f}(x) \oplus z^*_{s,f}(x)}{N-|m|}$$

and $\oplus$ denotes an operation of symmetric difference.

4.2 ENROLLEMENT

Typically, biometric systems require more than one measurement of the biometric specimen. This is common procedure that aims at compensating natural smoothness of biometric attributes, but also reducing the influence of variable conditions of the capturing process. The pattern of the human iris is a stable object, in contrast to (for instance) a handwritten signature. Thus, theoretically, only one iris image may be employed for template creation. However, both the eyeball rotation and pupil size are uncontrollable factors in iris imaging. Although the pupil size is compensated for by using a polar coordinate system to represent the iris sectors regardless of the pupil size, this transformation is linear, i.e. it maps the pupil constrictions and dilations linearly to the resulting polar representation. The iris is *de facto* a three-dimensional meshwork, and what one may observe is a warped two-dimensional projection of the three-dimensional

structure which may change nonlinearly with pupil constriction and dilation. Consequently, we employ at least three iris images at the enrollment stage.

In our approach, the iris template consists of features and the weights calculated for each f-stripe independently. We assume that the iris template may consist of features originating from f-stripes of different images of the same eye. This allows selecting the best representatives among more than one iris image, thus compensating for a noise and the iris body disruptions caused by elastic iris constrictions and dilations. A set of features belonging to a single f-stripe is additionally completed by a weight that points the significance of the corresponding f-stripe from identity recognition point o view. The selection of appropriate f-stripes, along with the corresponding weights, is a crucial operation and we briefly describe the proposed method.

The best f-stripe, hence a set of corresponding features that are incorporated into the template, is chosen using max-min method. A set of f-stripes originating from different images of the same eye can be represent as nodes of a graph, where the connections among the nodes represent the partial matching score $S_{s,f}$ (either $S_{s,f} = S^{rect}_{s,f}$ or $S_{s,f} = S^{sign}_{s,f}$), Fig. 7. Note, that having $8R$ f-stripes, we have to construct $8R$ such graphs.

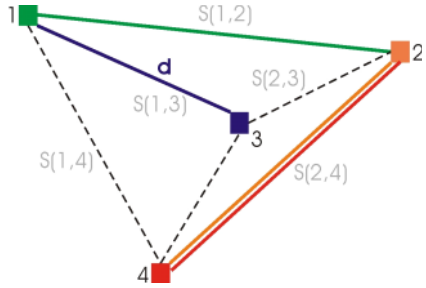

Figure 7. Selecting the best representative and the minimal distance

For each node k we record the maximal matching score $S^*_{s,f}(k) = \max_n(S_{s,f}(k,n))$. Then we incorporate to the template the f-stripe for which $S^*_{s,f}(k)$ in minimal with respect to k. We record $d_{s,f} = \min_k (S^*_{s,f}(k))$, and use $d_{s,f}$ to calculate the weight $w_{s,f}$. The smaller $d_{s,f}$, the more stable and noise insensitive f-stripe is incorporated to the template calculation. Consequently, we define weights $w_{s,f}$ as

$$w_{s,f} = \frac{\tilde{w}_{s,f}}{\sqrt{\sum_{s^*,f^*} \tilde{w}^2_{s^*,f^*}}} \tag{4.3}$$

where

$$\tilde{w}_{s,f} = \frac{1}{d_{s,f} + \epsilon} \tag{4.4}$$

and ε parameter is the uncertainty interval and it prevents from the degradation of the feature set size due to small value of matching score for a certain f-stripe.

It is noteworthy that our approach to template generation, in which each stripe is analyzed independently, partially compensates for non-linear iris pattern deformations due to the iris muscle stretching and shrinking.

4.2 VERIFICATION

The verification process employs the overall matching score $S(t,v)$ between the template t and the verification sample v. $S(t,v)$ is the weighted sum of the partial matching scores $S_{s,f}$, namely

$$S(t,v) = \sum_{s,f} w_{s,f} S_{s,f}(t,v) \tag{4.5}$$

The iris image is considered to be a genuine when the matching score $S(t,v)$ exceeds an acceptance threshold set experimentally with the use of local iris image database.

5. RECOGNITION RESULTS

For the purpose of testing we use iris images collected for 180 different eyes, and we have 4 images for one eye. The set of images were divided to two subsets: 3 iris images for each eye were taken to create templates, and the one image, unknown at the enrollment stage, is used in verification. We perform two kinds of comparisons. In the first we match each template with the image originating from the same class (genuine tries), receiving 180 comparison results. In the second phase we match each template with test image coming from different class, receiving 32 220 comparison results (impostor tries). Both matching score distributions are illustrated in Fig. 8 and 9, for method variants employing rectangular and sign-only representations, respectively.

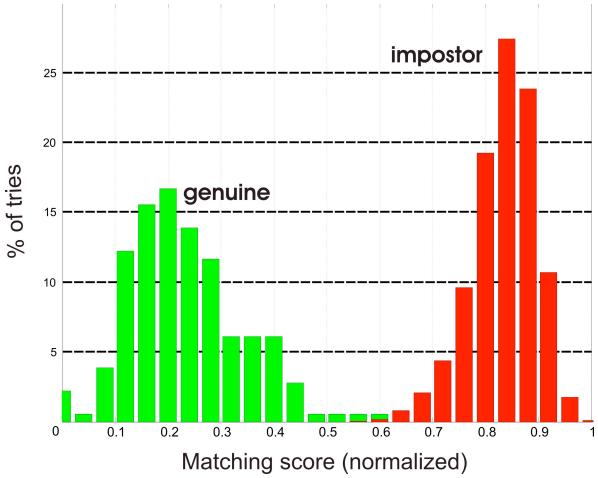

Figure 8 Score distributions for impostor and genuine comparisons for the *rectangular* representation of f-stripes.

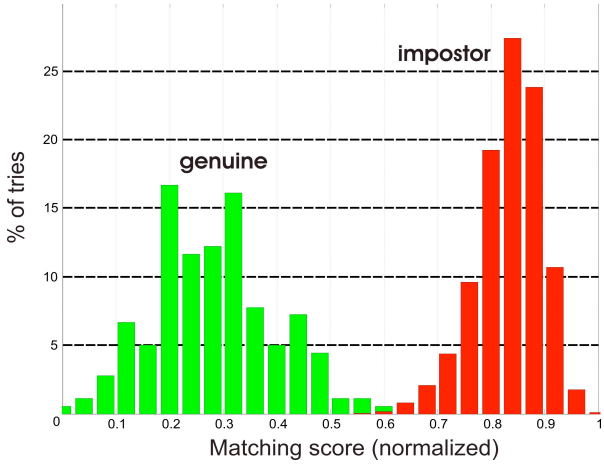

Figure 9 Same as in Fig. 8, except the *sign-only* representation of f-stripes.

To evaluate the method's strength, we consider a few typical measures.

Error measures Typically in biometrics we may expect two main errors: false acceptance or false rejection. We cannot determine the exact values of those error probabilities, yet they may be estimated with a finite set of comparison results. We use first-order approximation to form the estimators of error functions that results in piecewise linear functions of the decision threshold. Consequently, resulting approximations of false acceptance and false rejection errors are FAR (False Acceptance Rate) and FRR (False Rejection Rate), respectively. The ordinate of the crossing point of FAR and FRR is called ERR (Equal Error Rate). FAR and FRR, as a function of a decision threshold are depicted in Figure 10 and 11, again for both variants of zero-crossing method, employing rectangular and sign-only representations, respectively. We set the acceptance threshold as the abscissa of EER.

Separation measure Decidability coefficient d is a typical measure for iris biometrics performance evaluation. It measures how well the distributions of genuine and impostor comparisons are separated with respect to the overall matching score variability. It means the higher d the lower distributions overlap. It is defined as:

$$d = \frac{|m_X - m_Y|}{\sqrt{\frac{\sigma_X^2 + \sigma_Y^2}{2}}} \tag{6}$$

where m_X and m_Y are mean values of the matching score for genuine and impostor tries, σ_X and σ_Y are sample variances of matching scores for genuine and impostor tries, respectively.

Both algorithms achieved similar results in terms of d with a little advantage of coding that employs rectangular representation (d=6,08) over the sign-only representation (d=5,86). In turn, the proposed compact coding achieved better error rate (0.03%) than the approach (0.56%) employing the coding originally inspired by Boles' works. Table 1 presents values of all the measures for both variants of the approach.

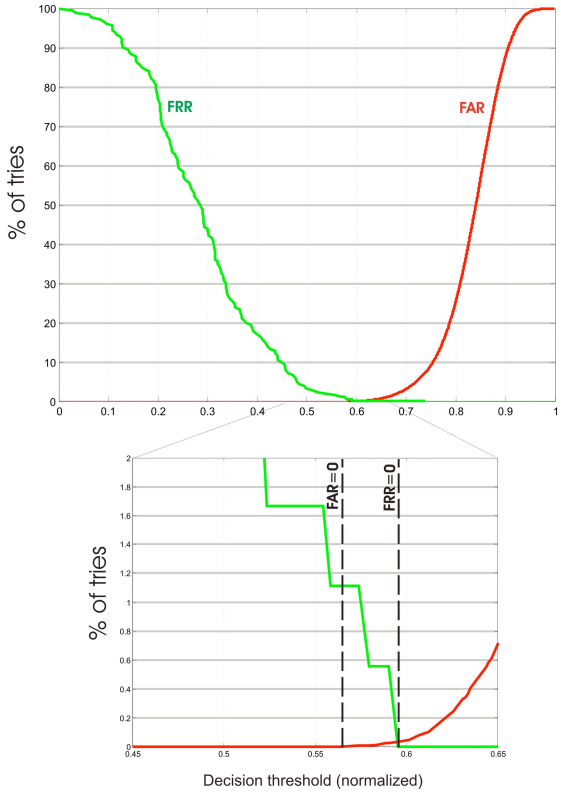

Figure 10 FAR-FRR curves for the *sign-only* representation. EER = 0.03%.

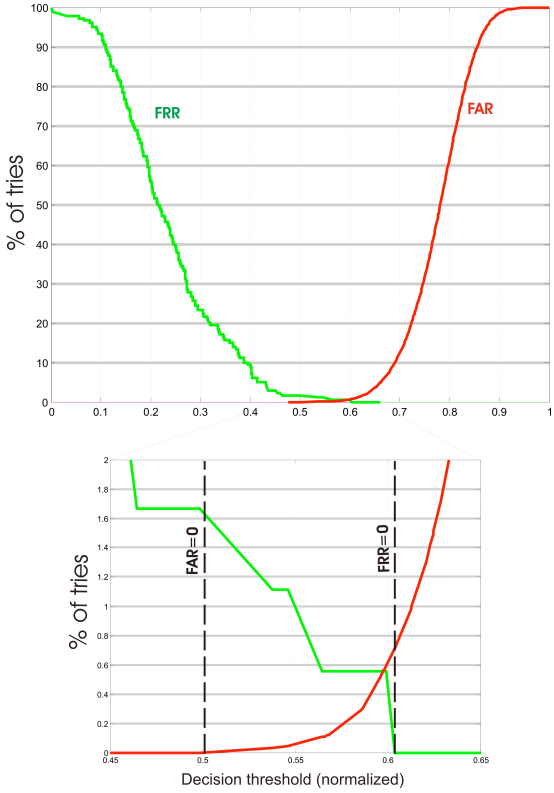

Figure 11 Same as in Fig. 10, except the results for *rectangular* representation is illustrated. EER = 0.56%.

Table 1. Results for both variants of zero-crossing based coding for a database of 180 different eyes

Coding	**EER**	**FAR for FRR=0**	**FRR for FAR=0**	**d (decidability)**
Rectangular	0.56%	0,7%	1,62%	6,08
Sign-only	0.03%	0,032%	1,1%	5,86

5. SUMMARY

We described an iris recognition technique using a zero-crossing-based coding obtained by filtering the iris image by way of Laplacian of Gaussians. The entire process of iris recognition is depicted, starting from image acquisition, ending up with an identity verification decision. To achieve this, iris localization and occlusion detection methods are described, that result in representation the iris image in a form of sequence of 1D stripes. We proposed the enrollment procedure that relies on an independent selection of iris stripes among a number of enrollment images to minimize the recognition errors. Additionally, the eyeball spontaneous rotation is corrected at the verification stage.

Tests performed with a local database of iris images taken for 180 different proved that new simplified method of original zero-crossing-based feature coding not only significantly reduces the size of the feature vector but also sustain the comparable level of performance, or even overtake the original method in terms of EER (at the level of 0.03%).

The proposed approach is computationally very fast. It is also noteworthy that the representation and a matching in the case of using sign-only representation is a very promising method for the computation constrained environments such as smart card or microelectronic devices.

REFERENCES

1. American National Standards Institute, “Information technology — Biometric data interchange formats — Part 6: Iris image data”, ISO/IEC JTC 1, Final Draft International Standard (FDIS) 19794-6:2005(E), 2005
2. W. W. Boles, “A Security System Based on Human Iris Identification Using Wavelet Transform", *Knowledge-Based Intelligent Electronic Systems, KES'97. Proceedings. First International Conference on*, Adelaide, Australia, pp. 533-541, Vol. 2, 1997
3. John Daugman, “Biometric personal identification system based on iris analysis”, *United States Patent US 5,291,560*, assignee: IriScan Inc., NJ, USA, March 1, 1994
4. John Daugman, “How Iris Recognition Works”, *IEEE Transactions on Circuits and Systems for Video Technology*, Vol. 14, No. 1, January 2004
5. Li Ma, Tieniu Tan, Yunhong Wang, Dexin Zhang, “Efficient iris recognition by characterizing key local variations”, *Image Processing, IEEE Transactions on*, Vol. 13, Issue 6, pp. 739 - 750, June 2004
6. Andrzej Pacut, Adam Czajka, Przemek Strzelczyk, “Iris biometrics for secure remote access”, in: J.S. Kowalik *et al.* (Eds.), *Cyberspace Security and Defense: Research Issues*, pp. 259-278, Springer, 2005
7. Przemysław Strzelczyk, “Zastosowanie biometrii tęczówki oka w systemach uwierzytelniających”, Master Thesis, Institute of Control and Computation Engineering, Warsaw University of Technology, 2005